

Turbulent dynamos in a collapsing cloud

Muhammed Irshad P,^{1,*} Pallavi Bhat,¹ Kandaswamy Subramanian,^{2,3} and Anvar Shukurov⁴

¹International Centre for Theoretical Sciences, Tata Institute of Fundamental Research, Bangalore 560089, India

²Inter-University Centre for Astronomy and Astrophysics, Post Bag 4, Ganeshkhind, Pune 411007, India

³Department of Physics, Ashoka University, Rajiv Gandhi Education City, Rai, Sonapat 131029, India

⁴School of Mathematics, Statistics and Physics, Newcastle University, Newcastle upon Tyne, NE1 7RU, U.K.

The amplification of magnetic fields is crucial for understanding the observed magnetization of stars and galaxies. Turbulent dynamo is the primary mechanism responsible for that but the understanding of its action in a collapsing environment is still rudimentary and relies on limited numerical experiments. We develop an analytical framework and perform numerical simulations to investigate the behavior of small-scale and large-scale dynamos in a collapsing turbulent cloud. This approach is also applicable to expanding environments and facilitates the application of standard dynamo theory to evolving systems. Using a supercomoving formulation of the magnetohydrodynamic (MHD) equations, we demonstrate that dynamo action in a collapsing background leads to a *super-exponential* growth of magnetic fields in time, significantly faster than the exponential growth seen in stationary turbulence. The enhancement is mainly due to the increasing eddy turnover rate during the collapse, which boosts the instantaneous growth rate of the dynamo. We also show that the final saturated magnetic field strength exceeds the expectation from considerations of pure flux-freezing or energy equipartition with the turbulence, scaling as $B \propto \rho^{5/6}$, where ρ is the cloud density. Apart from establishing a formal framework for the studies of magnetic field evolution in collapsing (or expanding) turbulent plasmas, these findings have significant implications for early star and galaxy formation, suggesting that magnetic fields can be amplified to dynamically relevant strengths much earlier than previously thought.

INTRODUCTION

Coherent and random magnetic fields are both ubiquitous in stars and galaxies [1–4]. The leading paradigm that has the potential to explain the origin of these magnetic fields is the turbulent dynamo theory [5, 6]. In a highly conducting turbulent plasma, the *small-scale dynamo* (SSD) amplifies magnetic fluctuations on a typical time scale of order the turnover time of a turbulent eddy, whereas the *large-scale dynamo* (LSD) generates fields coherent on scales larger than the turbulent scale on a longer time scale. In galaxies, the two time scales are of order 10 Myr and 5–10 Gyr, respectively. In protostellar environments, these estimates are less general but the difference in the time scales remains significant.

Moreover, magnetic fields coherent on scales of a few kiloparsecs appear to be present in galactic and protogalactic environments even at high redshifts [7–11]. Their amplification on the corresponding time scale of a few Gyr requires a special explanation as suggested here.

The early production of magnetic fields can have a significant impact on the formation of gas structures. Magnetic fields can hinder fragmentation, and thereby influence the stellar initial mass function [12–14]. Sufficiently strong magnetic fields can facilitate the formation of jets and outflows from accretion disks [15, 16] removing a significant fraction of mass and angular momentum and thus affecting the stellar mass spectrum [17]. Magnetic fields can influence the evolution of galaxies [18] and contribute to the feedback processes such as galactic winds and fountains [19, 20].

The formation of stars and galaxies starts with the collapse of a gas cloud driven by gravitational, thermal and other instabilities leading to turbulence [21–28]. The turbulence can be amplified during the gravitational contraction [29–36]. This

presents an intriguing possibility of the dynamo process receiving a boost from the collapse leading to an accelerated growth of magnetic fields. Previous analytical studies [37–40] did not account for this enhancement of the kinematic dynamo, assuming the kinematic regime to be much shorter than the free-fall time and instead focused on the nonlinear, steady-state dynamo regime [41–44]. Also, accelerated growth in numerical simulations can be difficult to detect without the right parameter regime and systematic comparisons across parameter variations.

In this letter, we develop an analytical framework for dynamo action in a collapsing cloud to demonstrate that dynamo action leads to a super-exponential growth of the magnetic field strength. Nonlinear regimes of magnetic field evolution in such environments are explored using numerical simulations.

COLLAPSE OF A HOMOGENEOUS CLOUD

Consider a turbulent cloud undergoing homologous collapse. The position of the fluid element and its density are given by,

$$\mathbf{r} = a(t)\mathbf{r}_c, \quad \rho(t) = \rho_c/a^3(t), \quad 0 < a(t) \leq 1, \quad (1)$$

where $a(t)$ is the scale factor determining the size, \mathbf{r}_c and ρ_c are the comoving position and density, respectively.

Even in the comoving coordinates, the magnetohydrodynamics (MHD) equations are still intricate because of the contribution from the background collapse to the total velocity of fluid element given by

$$\mathbf{u} = \mathbf{v} + H\mathbf{r}, \quad H = d \ln a/dt, \quad (2)$$

where \mathbf{v} is the peculiar velocity and $H\mathbf{r}$ is the velocity of the collapsing background. Following Ref. [45], we introduce the

so-called supercomoving variables denoted here with tilde,

$$\begin{aligned} \tilde{\mathbf{r}} &= \mathbf{r}/a, & d\tilde{t} &= dt/a^2, & \tilde{\rho}(\tilde{t}) &= a^3\rho(t), \\ \tilde{\mathbf{v}}(\tilde{t}) &= a\mathbf{v}(t), & \tilde{p}(\tilde{t}) &= a^5p(t), & \tilde{\mathbf{B}}(\tilde{t}) &= a^2\mathbf{B}(t), \end{aligned} \quad (3)$$

where p is the pressure and \mathbf{B} is the magnetic field. This results in a simpler structure of the governing equations. Note that we use the supercomoving time \tilde{t} instead of t in the analysis and the definition of $\tilde{\mathbf{v}}$ accounts for the evolution of peculiar velocity as $1/a$ in a homologous collapse [46]. Similarly, $\tilde{\mathbf{B}}$ is defined so that the magnetic field amplification via flux freezing, in proportion to $1/a^2$, due to the overall collapse is factored out. For an incompressible comoving flow, the MHD equations in supercomoving coordinates follow as

$$\tilde{\nabla} \cdot \tilde{\mathbf{v}} = 0, \quad (4)$$

$$\frac{\partial \tilde{\mathbf{v}}}{\partial \tilde{t}} + (\tilde{\mathbf{v}} \cdot \tilde{\nabla})\tilde{\mathbf{v}} = -\frac{\tilde{\nabla}\tilde{p}}{\tilde{\rho}} + \tilde{a}\frac{(\tilde{\nabla} \times \tilde{\mathbf{B}}) \times \tilde{\mathbf{B}}}{4\pi\tilde{\rho}} + \nu\tilde{\nabla}^2\tilde{\mathbf{v}}, \quad (5)$$

$$\frac{\partial \tilde{\mathbf{B}}}{\partial \tilde{t}} = \tilde{\nabla} \times (\tilde{\mathbf{v}} \times \tilde{\mathbf{B}}) + \eta\tilde{\nabla}^2\tilde{\mathbf{B}}, \quad \tilde{\nabla} \cdot \tilde{\mathbf{B}} = 0. \quad (6)$$

The gravitational term is balanced by the acceleration of the collapse and, thus, does not appear in the momentum equation. In physical variables, this system corresponds to an adiabatically collapsing sphere, as evident from the scaling of pressure and density in Eq. (3). These equations have the same form as the MHD equations in a stationary background except for the factor $\tilde{a}(\tilde{t})$ in the Lorentz force, and we note that $\tilde{a}(\tilde{t}) \equiv a(t)$. The major advantage of these variables is that the induction equation retains its form. This helps to extend the standard kinematic dynamo theory to a homologous collapsing background.

The form of $a(t)$ is governed by the Friedmann equation

$$\frac{\ddot{a}}{a} = -\frac{4\pi G}{3}\rho(t), \quad (7)$$

where the dot denotes the time derivative, which can be integrated with the free-fall initial conditions $a(0) = 1$, $\dot{a}(0) = 0$:

$$\arctan\left(\sqrt{(1-a)/a}\right) + \sqrt{a(1-a)} = kt, \quad (8)$$

where $k = \sqrt{8\pi G\tilde{\rho}/3}$. In the limit $a \rightarrow 0$, t tends to the free-fall time, $t_{\text{ff}} = \pi/(2k) = [3\pi/(32G\tilde{\rho})]^{1/2}$, which is inversely proportional to the initial density of the plasma. This solution also leads to the relation between t and \tilde{t} . Taking the differential of Eq. (8), we have $d\tilde{t} = dt/a^2 = -k^{-1}a^{-3/2}(1-a)^{-1/2} da$, which results in

$$\tilde{t} = \frac{2}{k} \sqrt{\frac{1-a}{a}} \equiv f(t), \quad (9)$$

where the constant of integration follows from the requirement that $\tilde{t} = 0$ at $a = 1$ and $t = 0$. Inverting Eq. (9) gives the scale factor in terms of \tilde{t} ,

$$\tilde{a}(\tilde{t}) = \frac{1}{1 + k^2\tilde{t}^2/4}. \quad (10)$$

Note that $a \rightarrow 0$, $t \rightarrow t_{\text{ff}}$ in the limit $\tilde{t} \rightarrow \infty$. Thus, we cannot track the collapse up to the singularity in terms of the supercomoving time. A fit for the scale factor (accurate within 2%) given by $a(t) = \left(1 - t^2/t_{\text{ff}}^2\right)^{2/3}$, shows that initially the collapse is slow but it accelerates to reach a singularity at $t = t_{\text{ff}}$ [47]. The gas pressure stops the collapse before a singular state is reached as the cloud becomes sufficiently inhomogeneous and spherical symmetry breaks [48]. Therefore, in the simulations discussed below, the collapse is only extended to a certain earlier time t_* , after which magnetic field continues evolving against a stationary background.

TURBULENT DYNAMOS IN A COLLAPSING BACKGROUND

In a stationary environment, the coefficients of the induction equation are independent of time, so dynamo action results in an exponentially fast amplification of an initial (weak) magnetic field at the expense of the kinetic energy of the plasma [49, 50]. The exponential growth continues until the Lorentz force becomes comparable to the forces driving the plasma flow; after that, the exponential growth saturates. Since the induction equation, Eq. (6) in the supercomoving variables has the same form as in a stationary background, the dynamo action causes an exponential amplification of \tilde{B} in terms of the time variable \tilde{t} ,

$$\tilde{B} \propto \exp(\tilde{\gamma}\tilde{t}). \quad (11)$$

In a dynamo-passive system, $\tilde{\gamma} < 0$ because of the magnetic diffusion, but the dynamo action results in $\tilde{\gamma} > 0$. Suitable expressions for the growth rate $\tilde{\gamma}$ of the turbulent dynamos (SSD and LSD) can be found in [51]. Using Eqs (3) and (9) for the relations of the supercomoving magnetic field and time to the physical ones, we obtain the corresponding magnetic field strength in the rest frame,

$$B \propto \frac{1}{a^2(t)} \exp\left(\int_0^t \frac{\tilde{\gamma} dt'}{a^2(t')}\right) = \frac{1}{a^2(t)} e^{\tilde{\gamma}f(t)}, \quad (12)$$

where the factor $1/a^2$ is due to the overall collapse and $\tilde{\gamma} = \text{const}$ for both SSD and LSD [51]. Instead of a constant growth rate in a stationary environment, the dynamo action in a collapsing background produces a growth rate increasing with time because of the factor $f(t)$ in the exponent. We refer to this regime as a *super-exponential* growth of the magnetic field. By the end of the kinematic regime, the Lorentz force affects the plasma flow and the magnetic field strength reaches a stationary saturation level. The magnetic energy density becomes comparable to the turbulent energy density,

$$\tilde{a}\tilde{B}^2/8\pi \simeq \frac{1}{2}\tilde{\rho}\tilde{v}^2 \quad (13)$$

in terms of the rms values of \tilde{B} and $\tilde{\rho}\tilde{v}^2$, where the factor \tilde{a} is due to the coefficient of the Lorentz force in Eq. (5). In terms

of the physical saturated magnetic field strength, assuming $\tilde{\rho}\tilde{v}^2 = \text{const}$, this implies

$$B \propto a^{-5/2} \propto \rho^{5/6}, \quad (14)$$

rather than just $a^{-2} \propto \rho^{2/3}$. An important implication of this scaling is that the saturated magnetic fields can significantly exceed the strength predicted by either flux-freezing alone or energy equipartition with the turbulence characteristic of the dynamo in a stationary background:

$$B^2/(8\pi) \simeq \frac{1}{2}\rho v^2 = a^{-5}\frac{1}{2}\tilde{\rho}\tilde{v}^2.$$

KINEMATIC DYNAMOS

To verify and refine the analytical arguments, we solved Eqs (4)–(6) numerically, with the induction equation written in terms of the vector potential.

A random flow at an energy-range scale \tilde{l}_0 is driven by a random force added on the right-hand side of the momentum equation, Eq. (5). We use the forcing function [52] from the PENCIL CODE [53], rewritten for the supercomoving coordinates (see [51]). The magnitude of the force driving the random flow is independent of the scale while the forcing wavenumbers $\tilde{\mathbf{k}}$ are random in direction and have magnitudes from the uniform distribution in the ranges $1 \leq \tilde{k} \leq 3$ (the average $\tilde{k}_0 = 2\pi/\tilde{l}_0 = 2$) for the SSD simulations and $3 \leq \tilde{k} \leq 5$ ($\tilde{k}_0 = 4$) for the LSD. Note that the forcing scale decreases with time in the rest frame [41].

The driving force is mirror-symmetric in the SSD simulations and helical when the LSD is considered. The resulting LSD is of the a^2 type because of the lack of differential rotation [54]. In differentially rotating clouds, the LSD can be significantly more efficient [6]. A random flow can be helical, and thus drive an LSD, in a rotating system. We neglect any deviation from spherical symmetry which may arise from the rotation.

We non-dimensionalize the equations with the forcing scale \tilde{l}_0 , the rms random speed \tilde{v}_0 (even in simulations without a forced random flow), and $\rho_0 = \tilde{\rho}_0$, the plasma density at $t = \tilde{t} = 0$. The corresponding unit time is $\tilde{t}_0 = \tilde{l}_0/\tilde{v}_0$ and the unit magnetic field is $\tilde{B}_0 = (4\pi\tilde{\rho}_0\tilde{v}_0^2)^{1/2}$. The corresponding kinetic and magnetic Reynolds numbers, $\text{Re} = \tilde{l}_0\tilde{v}_0/\nu$ and $R_m = \tilde{l}_0\tilde{v}_0/\eta$, are defined in the supercomoving variables and thus do not change with time. For illustration, $\tilde{t}_0 \simeq 10^8$ yr and $\tilde{B}_0 \simeq 4 \times 10^{-7}$ G for $\tilde{l}_0 = 100$ pc, $\tilde{v}_0 = 1$ km s $^{-1}$, and $\tilde{\rho}_0 = 10^{-24}$ g cm $^{-3}$, parameters often used in the simulations of primordial star formation [37].

We used the publicly available code DEDALUS [55], a pseudospectral solver for partial differential equations. The simulations were carried out in a periodic cubic box $(2\pi)^3$ in size, with a resolution of 128^3 . The initial vector potential is a random Gaussian noise with a strength 10^{-5} .

The kinetic and magnetic Reynolds numbers used are $\text{Re} = R_m = 415$ for the SSD simulations, while $\text{Re} = 180$ and $R_m = 18$ for the LSD. The smaller R_m in the latter case is chosen

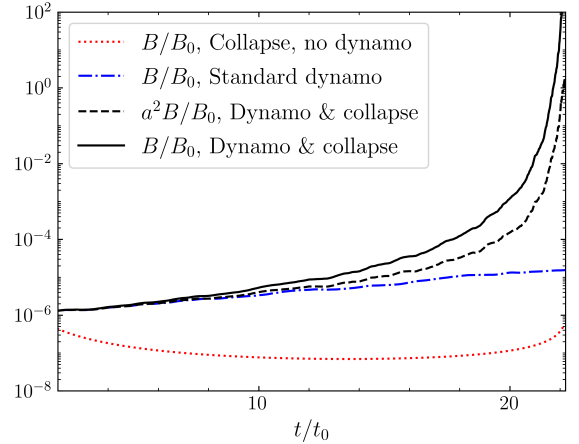


FIG. 1. Comparison of magnetic field evolution in SSD for different cases. Without collapse, there is exponential growth due to standard dynamo (dash-dotted). With collapse ($t_{\text{ff}} = 50$) and without forcing (dotted), there is no dynamo; flux freezing competes with resistive diffusion. With both collapse and forcing the dynamo grows the magnetic field super-exponentially (dashed), which is further enhanced by the collapse (solid). The dashed curve factors out the $1/a^2$ growth due to overall collapse and emphasizes on the super-exponential growth due to dynamo.

to support the LSD but not the SSD (which requires $R_m \gtrsim 100$ [56]), so that we can study the two dynamo mechanisms separately.

To reveal the effect of a collapsing background on dynamo action, we use three simulation runs for each of the SSD and LSD: (i) dynamo action in a stationary environment (referred to as the ‘standard’ dynamo) leading to an exponential magnetic field amplification, (ii) background collapse with $t_{\text{ff}} = 50$ without any random flow, thus no dynamo, and the magnetic field is only amplified due to magnetic flux freezing weakened by the magnetic diffusion, (iii) collapse with $t_{\text{ff}} = 50$ and driven random flow, so the magnetic field grows due to both dynamo action and the overall collapse of the plasma. The free-fall time chosen is shorter than the time at which the kinematic regime ends for the standard dynamo, t_{nl} (which depends on the seed magnetic field strength and the dynamo amplification time scale).

Figures 1 and 2 show the magnetic field evolution in the SSD and LSD, respectively, in the three scenarios. The collapse-induced compression of the magnetic field slows its resistive decay (dotted curves). When the magnetic diffusivity is relatively small ($R_m = 415$, Fig. 1), the compression becomes stronger than the decay at the final, accelerated stages of the collapse and the magnetic field strength slightly increases. However, the decay (which is also super-exponential) dominates at all times when the diffusivity is larger, $R_m = 18$ (Fig. 2). But, the magnetic field in a collapsing turbulent flow is both compressed by the overall collapse (approximately as $\propto a^{-2}$) and amplified by dynamo action. The contribution of the dynamo is isolated in $a^2 B$ (dashed), and $\log(a^2 B)$ increases faster than

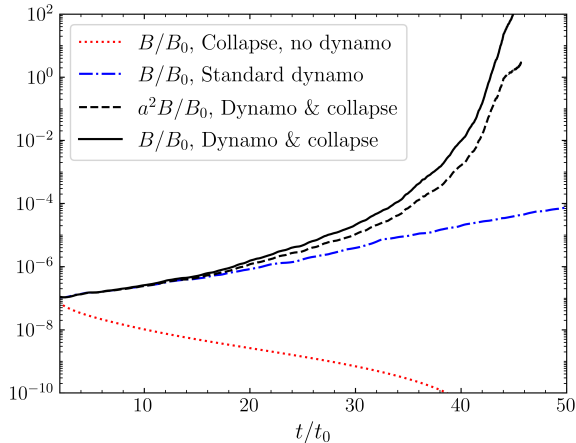


FIG. 2. As Fig. 1 but for the LSD with $\text{Re} = 180$ and $R_m = 18$.

t showing its super-exponential growth. This confirms that the instantaneous growth rates of both types of the dynamo, SSD and LSD, increase during the collapse. The solid lines in Figs 1 and 2 show the evolution of the physical magnetic field strength confirming that is indeed strongly super-exponential.

NONLINEAR DYNAMOS

To investigate the nonlinear dynamos numerically, we stop the collapse at a certain time t_* well before the singular state is reached. After that, the scale factor remains constant at a_* . If t_* occurs in the kinematic dynamo stage, the magnetic field continues growing exponentially (without acceleration) until the saturation. We also considered cases where the dynamo is already in the nonlinear stage at t_* . Thus, Eq. (10) is modified as

$$\tilde{a}(\tilde{t}) = \begin{cases} (1 + k^2\tilde{t}^2/4)^{-1} & \text{if } \tilde{t} \leq \tilde{t}_*, \\ (1 + k^2\tilde{t}_*^2/4)^{-1} & \text{if } \tilde{t} > \tilde{t}_*. \end{cases} \quad (15)$$

The resulting discontinuity in the time derivative of \tilde{a} leads to a discontinuity in the time variation of the Lorentz force. Therefore, the transition to a constant \tilde{a} was smoothed about $\tilde{t} = \tilde{t}_*$ using a moving average. To convert the supercomoving time \tilde{t} to the real time t , we numerically integrate $d\tilde{t} = dt/a^2$ given in Eq. (3) using Eq. (15). We use a_* in the range 0.1–1 because smaller values require very long simulation runs.

The rate at which magnetic field is amplified in the kinematic dynamo stage depends on both the free-fall time t_{ff} (thus on the initial cloud density) and the time when the collapse stops, i.e., on a_* (if the dynamo is still kinematic at t_*), whereas the steady-state magnetic field strength depends only on a_* . We consider three cases where t_{ff} is smaller, comparable to or larger than the time t_{nl} when the standard dynamo becomes nonlinear and the magnetic field growth saturates to reach a quasi-steady state (note that t_{nl} is different for the SSD and

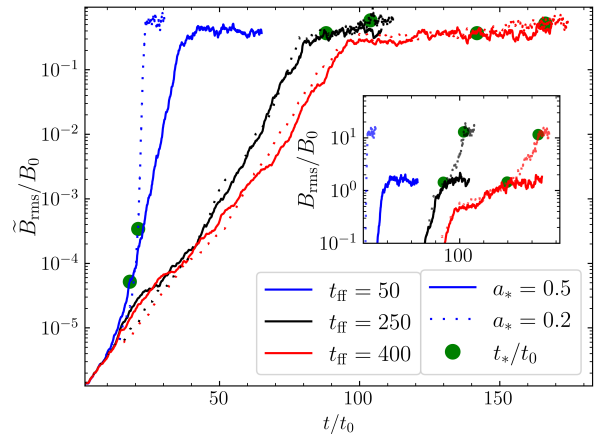


FIG. 3. The rms supercomoving magnetic field strength compensated for the compression, $\tilde{B}_{\text{rms}}/B_0$, in the SSD, for various values of t_{ff} . The solid and dotted curves represent two choices of the scale factor at which the collapse ends, $a_* = 0.5$ and 0.2 , respectively. The inset plot presents the physical B_{rms} focusing on the nonlinear stage. The green dots on the curves represent the point at which the collapse has been stopped. The blue curves correspond to $t_{\text{ff}} < t_{\text{nl}}$ and the others to $t_{\text{ff}} \gtrsim t_{\text{nl}}$.

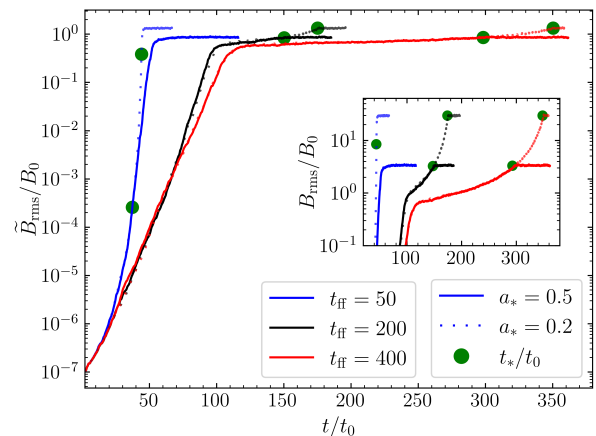


FIG. 4. As Fig. 3 but for the LSD.

LSD): (i) $t_{\text{nl}} > t_{\text{ff}} = 50$, (ii) $t_{\text{nl}} \sim t_{\text{ff}} = 250$ (SSD), 200 (LSD), (iii) $t_{\text{nl}} < t_{\text{ff}} = 400$. In all cases, we stop the collapse at two different times, $t_*/t_{\text{ff}} = 0.8$ and 0.95 which correspond to different simulations with $a_* \simeq 0.5$ and 0.2 , respectively.

Figures 3 and 4 show the evolution of magnetic field in the SSD and LSD, respectively. The main frames isolate the effect of the dynamo action on the supercomoving rms magnetic field strength (presenting $\tilde{B}_{\text{rms}} = a^2 B_{\text{rms}}$) whereas the insets, focusing on the nonlinear regime, show how the physical rms magnetic field B_{rms} grows due to both compression and dynamo action. As Eqs. (10) and (12) show, when t_{ff} is smaller (the cloud is denser), \tilde{a} evolves faster and the mag-

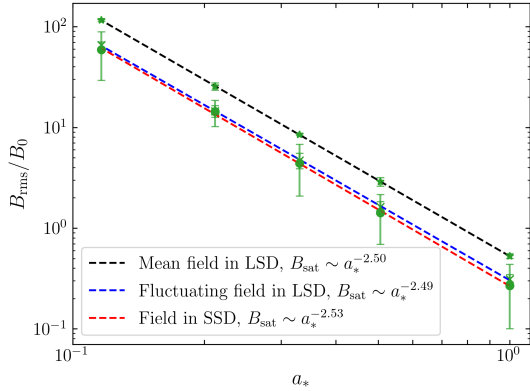


FIG. 5. The dependence of the saturated rms strength of the physical magnetic field on a_* for $t_{\text{ff}} = 50$. The error bars show the 5σ deviation. The dashed lines show the scaling of Eq. (13).

netic field grows correspondingly faster in its kinematic stage. An important observation is the distinction in magnetic field evolution between the cases where $t_{\text{ff}} < t_{\text{nl}}$ and $t_{\text{ff}} \gtrsim t_{\text{nl}}$. To appreciate this, we note that in the stationary background the kinematic stage ends (and the magnetic field strength levels off) at $t_{\text{nl}} = 250$ and 200 in the SSD and LSD, respectively, significantly later than in a collapsing cloud with $t_{\text{ff}} < t_{\text{nl}}$. As a result, denser clouds develop strong magnetic fields earlier. Furthermore, if the dynamos were inefficient in a stationary background, the collapse would help it to reach the end of the kinematic regime *much* faster. This kind of speed-up is less significant when $t_{\text{ff}} \gtrsim t_{\text{nl}}$.

The supercomoving magnetic field continues to grow in the nonlinear regime in line with Eq. (13) which shows that $\tilde{B} \propto \tilde{a}(\tilde{t})^{-1/2}$ arising from the weakening of the supercomoving Lorentz force. The physical field also grows due to the flux freezing as shown in Eq. (14). Despite a strong effect of the collapse on the kinematic dynamo, the saturated magnetic field strength is virtually independent of t_{ff} but is sensitive to the degree of compression, a_* . Figure 5 shows the saturated physical field strength as a function of a_* . In a remarkable agreement with Eq. (14), B_{rms} scales as $a_*^{-5/2}$. We note that the magnetic field \mathbf{B} is random with vanishing mean value in the case of the SSD and has a significant mean component in the LSD. As shown in Fig. 5, both parts of the magnetic field in the LSD scale similarly with a_* .

CONCLUSIONS AND DISCUSSION

Dynamo action in a stationary environment leads to an exponentially fast amplification of a seed magnetic field. We have shown that in a collapsing cloud the dynamo leads to a faster, super-exponential growth of the magnetic field. This effect is stronger than just a superposition of compression and exponential growth: the variable $a^2 B$, where the overall impact

of compression is factored out, also grows super-exponentially because the instantaneous growth rate of the magnetic field increases in the course of the collapse. The analysis in this work has benefited from using a framework of supercomoving variables that allowed us to recover the MHD equations in the collapsing background in nearly their original form.

Apart from the effect on the rate of amplification, the collapse also enhances the steady-state strength of the magnetic field which scales with the scale factor a as $B \propto a^{-5/2}$, as opposed to $B \propto a^{-2}$ for a frozen-in magnetic field. For a spherically-symmetric collapse, a frozen-in magnetic field increases with the gas density ρ as $B \propto \rho^{2/3}$, whereas the dynamo action leads to $B \propto \rho^{5/6}$. Galaxies form from the intergalactic medium with a density enhancement by a factor of 10^5 – 10^6 . Without any dynamo action, a frozen-in magnetic field would evolve from an initial value B_i to $(\rho/\rho_0)^{2/3} B_i \approx 10^4 B_i$. However, with a dynamo operating, the final field strength, in equipartition with the turbulent flow, is $10^5 (4\pi\rho_0 v_0^2)^{1/2}$, where $(\rho/\rho_0)^{5/6} \approx 10^5$. This is significantly stronger than what is achieved by flux-freezing alone or by a standard dynamo without collapse. The contributions from the dynamo and flux-freezing (on top of the dynamo) can be separated, with the latter providing the dominant enhancement. We have discussed these effects using the standard turbulent dynamos which generate random (SSD) and large-scale (LSD) magnetic fields, but the analysis applies to any other fast dynamo.

The super-exponential growth of both random and mean magnetic fields in a collapsing turbulent cloud could significantly alter estimates of the age at which young galaxies develop observable magnetic fields. Current dynamo models which do not include this effect explain large-scale magnetic fields at the redshift $z \approx 3$ [57, 58], whereas random magnetic fields can become significant even earlier. Ordered galactic magnetic fields have been reported at redshifts up to $z = 2.6$ [59] and even $z = 5.6$ [11]. The polarized dust emission detected can emerge from both anisotropic random magnetic fields (which naturally occur in spiral arms due to differential rotation [6]) and mean magnetic fields. Whatever is the nature of the galactic magnetic fields at high redshifts, its super-exponential amplification may be a crucial aspect of the theory. To illustrate the new opportunities, we note that, in the case $t_{\text{ff}} \sim 0.1 t_{\text{nl}}$, where t_{nl} marks field saturation at presumably an observable strength, the super-exponential growth over 15 orders of magnitude reduces t_{nl} of the standard dynamo by a factor of 10 [51], significantly affecting our understanding of galactic magnetic fields at high redshifts [60]. Cosmological MHD simulations of galaxy formation suggest turbulent dynamo action [61, 62], but evidence for super-exponential growth—potentially a key dynamo signature in a collapsing environment—has yet to be presented.

Our results also apply to primordial star formation, leading to significantly stronger protostellar magnetic fields [41]. The average gas density in stars (of the order 10^{24} cm^{-3}) is much higher than that of molecular clouds (of order 10^3 cm^{-3}) from which they form. Thus the compression factor is enormous. However, it is possible that the dynamo is inefficient in these

environments due to a low Prandtl number or low ionization, leading to a very large t_{nl} . Even then the collapse can significantly enhance the dynamo, with the extent of the speed-up depending on how large the ratio t_{nl}/t_{ff} is. A more detailed calculation of both the speed-up timescales and saturated magnetic field strengths in early stars and galaxies will be presented in a future work.

In general, local vortical motions in turbulent flows are amplified during any collapse (because of the specific angular momentum conservation), leading to faster eddy turnover time and larger dynamo growth rate. The results obtained here in the context of homologous collapse can be adapted to any mode of the collapse (e.g., the hierarchical collapse [48, 63]). In particular, the conclusion that dynamo action leads to a super-exponential amplification of the magnetic field applies to any collapsing system.

ACKNOWLEDGMENTS

We thank Godwin Martin and the members of the ICTS Plasma - Astrophysics group, particularly Vinay Kumar, for useful discussions. This research was supported by the Department of Atomic Energy, Government of India, under Project No. RTI4001. All simulations were performed on the Contra computing cluster at the International Centre for Theoretical Sciences, Tata Institute of Fundamental Research.

* muhammed.irshad@icts.res.in

- [1] A. Reiners, *Living Rev. Solar Phys.* **9**, 1 (2012).
- [2] C. L. H. Hull and Q. Zhang, *Front. Astron. Space Sci.* **6** (2019).
- [3] R. Beck, *Astron. Astrophys. Rev.* **24**, 4 (2015).
- [4] A. S. Borlaff, E. Lopez-Rodriguez, R. Beck, S. E. Clark, E. Ntormousi, K. Tassis, S. Martin-Alvarez, M. Tahani, D. A. Dale, I. del Moral-Castro, J. Roman-Duval, P. M. Marcum, J. E. Beckman, K. Subramanian, S. Eftekharzadeh, and L. Proudfit, *Astrophys. J.* **952**, 4 (2023).
- [5] A. Brandenburg and K. Subramanian, *Phys. Rep.* **417**, 1 (2005).
- [6] A. Shukurov and K. Subramanian, *Astrophysical Magnetic Fields: From Galaxies to the Early Universe* (Cambridge University Press, Cambridge, 2021).
- [7] M. L. Bernet, F. Miniati, S. J. Lilly, P. P. Kronberg, and M. Dessauges-Zavadsky, *Nature* **454**, 302 (2008).
- [8] J. S. Farnes, S. P. O'Sullivan, M. E. Corrigán, and B. M. Gaensler, *Astrophys. J.* **795**, 63 (2014).
- [9] J. S. Farnes, L. Rudnick, B. M. Gaensler, M. Haverkorn, S. P. O'Sullivan, and S. J. Curran, *Astrophys. J.* **841**, 67 (2017).
- [10] S. A. Mao, C. Carilli, B. M. Gaensler, O. Wucknitz, C. Keeton, A. Basu, R. Beck, P. P. Kronberg, and E. Zweibel, *Nat. Astron.* **1**, 621 (2017).
- [11] J. Chen, E. Lopez-Rodriguez, R. J. Ivison, J. E. Geach, S. Dye, X. Liu, and G. Bendo, *Astron. Astrophys.* **692**, A34 (2024).
- [12] Joos, M., Hennebelle, P., Ciardi, A., and Fromang, S., *Astron. Astrophys.* **554**, A17 (2013).
- [13] M. R. Krumholz and C. Federrath, *Front. Astron. Space Sci.* **6**, 7 (2019).
- [14] P. Hennebelle, U. Lebreuilly, T. Colman, D. Elia, G. Fuller, S. Leurini, T. Nony, E. Schisano, J. D. Soler, A. Traficante, R. S. Klessen, S. Molinari, and L. Testi, *Astron. Astrophys.* **668**, A147 (2022).
- [15] R. Banerjee and R. E. Pudritz, *Astrophys. J.* **641**, 949 (2006).
- [16] T. P. Ray and J. Ferreira, *New Astron. Rev.* **93**, 101615 (2021).
- [17] Lebreuilly, U., Hennebelle, P., Maury, A., González, M., Traficante, A., Klessen, R., Testi, L., and Molinari, S., *Astron. Astrophys.* **683**, A13 (2024).
- [18] M. Sanati, S. Martin-Alvarez, J. Schober, Y. Revaz, A. Slyz, and J. Devriendt, *Astron. Astrophys.* **690**, A59 (2024).
- [19] R. E. Pudritz, M. J. Hardcastle, and D. C. Gabuzda, *Space Sci. Rev.* **169**, 27 (2012).
- [20] E. Ntormousi, *Astron. Astrophys.* **619**, L5 (2018).
- [21] B. W. O'Shea and M. L. Norman, *Astrophys. J.* **654**, 66 (2007).
- [22] T. H. Greif, J. L. Johnson, R. S. Klessen, and V. Bromm, *Mon. Not. R. Astron. Soc.* **387**, 1021 (2008).
- [23] N. Yoshida, K. Omukai, and L. Hernquist, *Science* **321**, 669–671 (2008).
- [24] R. S. Klessen and P. Hennebelle, *Astron. Astrophys.* **520**, A17 (2010).
- [25] M. J. Turk, J. S. Oishi, T. Abel, and G. L. Bryan, *Astrophys. J.* **745**, 154 (2012).
- [26] E. J. Lee, P. Chang, and N. Murray, *Astrophys. J.* **800**, 49 (2015).
- [27] Y. Hu, A. Lazarian, and S. Stanimirović, *Astrophys. J.* **912**, 2 (2021).
- [28] A. Soam, C. Eswaraiyah, A. Seta, L. Dewangan, and G. Maheswar, *J. Astrophys. Astron.* **45**, 17 (2024).
- [29] S. Higashi, H. Susa, and G. Chiaki, *Astrophys. J.* **915**, 107 (2021).
- [30] S. Higashi, H. Susa, and G. Chiaki, *Astrophys. J.* **940**, 38 (2022).
- [31] E. Vázquez-Semadeni, J. Cantó, and S. Lizano, *Astrophys. J.* **492**, 596 (1998).
- [32] Y. Birnboim, C. Federrath, and M. Krumholz, *Mon. Not. R. Astron. Soc.* **473**, 2144 (2017).
- [33] B. Robertson and P. Goldreich, *Astrophys. J. Lett.* **750**, L31 (2012).
- [34] A. Mandal, C. Federrath, and B. Körtgen, *Mon. Not. R. Astron. Soc.* **493**, 3098 (2020).
- [35] P. Hennebelle, *Astron. Astrophys.* **655**, A3 (2021).
- [36] S. Xu and A. Lazarian, *Astrophys. J.* **890**, 157 (2020).
- [37] C. F. McKee, A. Stacy, and P. S. Li, *Mon. Not. R. Astron. Soc.* **496**, 5528 (2020).
- [38] S. Xu and A. Lazarian, *Astrophys. J.* **899**, 115 (2020).
- [39] A. Brandenburg and E. Ntormousi, *Mon. Not. R. Astron. Soc.* **513**, 2136 (2022).
- [40] S. Higashi, H. Susa, C. Federrath, and G. Chiaki, *Astrophys. J.* **962**, 158 (2024).
- [41] S. Sur, D. R. G. Schleicher, R. Banerjee, C. Federrath, and R. S. Klessen, *Astrophys. J. Lett.* **721**, L134 (2010).
- [42] C. Federrath, S. Sur, D. R. G. Schleicher, R. Banerjee, and R. S. Klessen, *Astrophys. J.* **731**, 62 (2011).
- [43] S. Sur, C. Federrath, D. R. G. Schleicher, R. Banerjee, and R. S. Klessen, *Mon. Not. R. Astron. Soc.* **423**, 3148 (2012).
- [44] A. Stacy, C. F. McKee, A. T. Lee, R. I. Klein, and P. S. Li, *Mon. Not. R. Astron. Soc.* **511**, 5042 (2022).
- [45] H. Martel and P. R. Shapiro, *Mon. Not. R. Astron. Soc.* **297**, 467 (1998).
- [46] P. Peebles, *Principles of Physical Cosmology*, Vol. 99 (Princeton Univ. Press., 2019).
- [47] P. Girichidis, L. Konstandin, A. P. Whitworth, and R. S. Klessen, *Astrophys. J.* (2014).
- [48] E. Vázquez-Semadeni, A. Palau, J. Ballesteros-Paredes, G. C. Gómez, and M. Zamora-Avilés, *Mon. Not. R. Astron. Soc.* **490**,

3061 (2019).

- [49] A. P. Kazantsev, *Sov. Phys. JETP*. **26**, 1031 (1968).
- [50] K. Subramanian, *Phys. Rev. Lett.* **83**, 2957 (1999).
- [51] See Supplementary Material.
- [52] S. Candelaresi and A. Brandenburg, *Phys. Rev. E* **87** (2013).
- [53] P. C. Collaboration, A. Brandenburg, A. Johansen, P. Bourdin, W. Dobler, W. Lyra, M. Rheinhardt, S. Bingert, N. Haugen, A. Mee, F. Gent, N. Babkovskaia, C.-C. Yang, T. Heinemann, B. Dintrans, D. Mitra, S. Candelaresi, J. Warnecke, P. Käpylä, A. Schreiber, P. Chatterjee, and et al., *J. Open Source Softw.* **6**, 2807 (2021).
- [54] D. Sokoloff, A. Shukurov, and A. Ruzmaikin, *Geophys. Astrophys. Fluid Dyn.* **25**, 293 (1983).
- [55] K. J. Burns, G. M. Vasil, J. S. Oishi, D. Lecoanet, and B. P. Brown, *Phys. Rev. Res.* **2** (2020).
- [56] N. E. L. Haugen, A. Brandenburg, and W. Dobler, *Phys. Rev. E* **70**, 016308 (2004).
- [57] L. F. S. Rodrigues, L. Chamandy, A. Shukurov, C. M. Baugh, and A. R. Taylor, *Mon. Not. R. Astron. Soc.* **483**, 2424 (2019).
- [58] C. Jose, L. Chamandy, A. Shukurov, K. Subramanian, L. F. S. Rodrigues, and C. M. Baugh, *Mon. Not. R. Astron. Soc.* **532**, 1504 (2024).
- [59] W. de Roo, S. Vegetti, D. M. Powell, S. W. Ndiritu, R. Pakmor, and J. P. McKean, (2024), [arXiv:2412.08705](https://arxiv.org/abs/2412.08705).
- [60] G. Heald, S. A. Mao, V. Vacca, T. Akahori, A. Damas-Segovia, B. M. Gaensler, M. Hoeft, I. Agudo, A. Basu, R. Beck, M. Birkinshaw, A. Bonafede, T. L. Bourke, A. Bracco, E. Carretti, L. Feretti, J. M. Girart, F. Govoni, J. A. Green, J. Han, M. Haverkorn, C. Horellou, M. Johnston-Hollitt, R. Kothes, T. Landecker, B. Nikiel-Wroczyński, S. P. O’Sullivan, M. Padovani, F. Poidevin, L. Pratley, M. Regis, C. J. Riseley, T. Robishaw, L. Rudnick, C. Sobey, J. M. Stil, X. Sun, S. Sur, A. R. Taylor, A. Thomson, C. L. Van Eck, F. Vazza, J. L. West, and et al., *Galaxies* **8**, 53 (2020).
- [61] S. Martin-Alvarez, J. Devriendt, A. Slyz, and R. Teyssier, *Mon. Not. R. Astron. Soc.* **479**, 3343 (2018).
- [62] R. Pakmor, R. Bieri, F. van de Voort, M. Werhahn, A. Fattahi, T. Guillet, C. Pfrommer, V. Springel, and R. Y. Talbot, *Mon. Not. R. Astron. Soc.* **528**, 2308 (2024).
- [63] B. Thomasson, I. Joncour, E. Moraux, F. Motte, F. Louvet, M. González, and T. Nony, *Astron. Astrophys.* **689**, A133 (2024).
- [64] K. Subramanian, *Phys. Rev. Lett.* **83**, 2957 (1999).

Supplemental Material

DYNAMO EQUATIONS AND THEIR SOLUTIONS IN SUPERCOMOVING VARIABLES

The interaction between a collisional plasma flow and magnetic field is described by the equations of magnetohydrodynamics (MHD),

$$\frac{\partial \rho}{\partial t} + \nabla \cdot (\rho \mathbf{u}) = 0, \quad (1)$$

$$\frac{D\mathbf{u}}{Dt} = -\nabla\Phi - \frac{\nabla p}{\rho} + \frac{(\nabla \times \mathbf{B}) \times \mathbf{B}}{4\pi\rho} + \nu \nabla^2 \mathbf{u}, \quad (2)$$

$$\frac{\partial \mathbf{B}}{\partial t} = \nabla \times (\mathbf{u} \times \mathbf{B}) + \eta \nabla^2 \mathbf{B}, \quad \nabla \cdot \mathbf{B} = 0, \quad (3)$$

where $D/Dt = \partial/\partial t + (\mathbf{u} \cdot \nabla)$, \mathbf{u} , p , and ρ are the gas velocity, pressure and density, respectively, Φ is the gravitational potential, \mathbf{B} is the magnetic field, and ν and η are the kinematic viscosity and magnetic diffusivity, respectively. The equations are closed by relating the pressure and density with the help of an equation of state.

As shown in the main text, the induction equation does not change its algebraic form when written in supercomoving variables. In this section, we present its solutions in supercomoving variables.

The small-scale dynamo (SSD)

Kazantsev's solution of the induction equation for the correlation function of the magnetic field in a random flow [49] remains one of the most often used models of the SSD in a stationary background [6]. The model assumes incompressible, statistically isotropic and homogeneous, mirror-symmetric, δ -correlated in time Gaussian random velocity field. Consider such an incompressible supercomoving velocity field $\tilde{\mathbf{v}}(\tilde{\mathbf{x}}, \tilde{t})$ and its supercomoving correlation tensor $\tilde{T}_{ij}(\tilde{r})$,

$$\langle \tilde{v}_i(\tilde{\mathbf{x}}, \tilde{t}) \tilde{v}_j(\tilde{\mathbf{y}}, \tilde{s}) \rangle = \tilde{T}_{ij}(\tilde{r}) \delta(\tilde{t} - \tilde{s}), \quad (4)$$

where $\tilde{r} = |\tilde{\mathbf{x}} - \tilde{\mathbf{y}}|$ and we note that the velocity field is δ -correlated in both original and supercomoving variables. Since the continuity equation preserves its form when written in the supercomoving variables (Sect. 4.2 of Ref. [45]) and the gas density is assumed to be independent of position, $\tilde{\nabla} \cdot \tilde{\mathbf{v}} = 0$ implies that the flow is incompressible in the physical variables as well, $\nabla \cdot \mathbf{v} = 0$. The velocity correlation tensor can be represented in terms of the longitudinal and transverse parts, \tilde{T}_L and \tilde{T}_N , respectively, as $\tilde{T}_{ij} = (\delta_{ij} - \tilde{r}_i \tilde{r}_j / \tilde{r}^2) \tilde{T}_N + \tilde{r}_i \tilde{r}_j \tilde{T}_L / \tilde{r}^2$, where \tilde{T}_L and \tilde{T}_N are related to each other because of the flow incompressibility, similarly to the relation (8) for the magnetic field correlators.

To derive the correlation tensor in terms of the peculiar velocity, we use $\tilde{\mathbf{v}} = a\mathbf{v}$ and $\tilde{t} = f(t)$ in Eq. (4):

$$\langle a(t)v_i(t) a(s)v_j(s) \rangle = \tilde{T}_{ij}(\tilde{r}) \delta(f(t) - f(s)). \quad (5)$$

Since

$$\delta[g(t)] = \frac{\delta(t - t_0)}{|g'(t_0)|},$$

where t_0 is the root of $g(t)$ (i.e., $t = s$ in our case), and $d\tilde{t} = dt/a^2$, we obtain

$$\delta[f(t) - f(s)] = \frac{1}{f'(t)|_{t=s}} \delta(t - s) = a(s)^2 \delta(t - s),$$

implying that

$$\langle v_i(t)v_j(s) \rangle = \tilde{T}_{ij}(\tilde{r}) \delta(t - s). \quad (6)$$

Hence the peculiar velocity correlation tensor is δ -correlated in real time.

The magnetic field correlation tensor $\tilde{M}_{ij}(\tilde{r}, \tilde{t})$ cannot be assumed to be δ -correlated in time [6], and it has the form

$$\langle \tilde{B}_i(\tilde{\mathbf{x}}, \tilde{t}) \tilde{B}_j(\tilde{\mathbf{y}}, \tilde{t}) \rangle = \tilde{M}_{ij}(\tilde{r}, \tilde{t}). \quad (7)$$

Since $\nabla \cdot \tilde{\mathbf{B}} = 0$, the magnetic field correlation tensor \tilde{M}_{ij} can be written in terms of its longitudinal and transverse correlators \tilde{M}_L and \tilde{M}_N , $\tilde{M}_{ij} = (\delta_{ij} - \tilde{r}_i \tilde{r}_j / \tilde{r}^2) \tilde{M}_N + \tilde{r}_i \tilde{r}_j \tilde{M}_L / \tilde{r}^2$, which are related as

$$\tilde{M}_N = \frac{1}{2\tilde{r}} \frac{\partial}{\partial \tilde{r}} (\tilde{r}^2 \tilde{M}_L). \quad (8)$$

Since the supercomoving equations are similar to MHD equations in a stationary background, the derivation of the equation for the longitudinal magnetic correlator in Ref. [49] remains applicable, and we obtain

$$\frac{\partial \tilde{M}_L}{\partial \tilde{t}} = \frac{2}{\tilde{r}^4} \frac{\partial}{\partial \tilde{r}} \left(\tilde{r}^4 \tilde{\eta}_T \frac{\partial \tilde{M}_L}{\partial \tilde{r}} \right) + \tilde{G} \tilde{M}_L, \quad (9)$$

where

$$\tilde{G} = -4 \left[\frac{d}{d\tilde{r}} \left(\frac{\tilde{T}_N}{\tilde{r}} \right) + \frac{1}{\tilde{r}^2} \frac{d}{d\tilde{r}} (\tilde{r} \tilde{T}_L) \right]$$

is responsible for the magnetic field amplification and $\tilde{\eta}_T = \eta + \tilde{T}_L(0) - \tilde{T}_L(\tilde{r})$ represents the dissipation due to the electric resistivity and turbulent diffusion. This equation can be reduced to a Schrödinger-type equation and using its solution in the WKBJ approximation leads to [6, 64]

$$\tilde{B}_{\text{rms}} \propto \exp(\tilde{\gamma} \tilde{t}), \quad \tilde{\gamma} \simeq \tilde{v}_0 / \tilde{l}_0, \quad (10)$$

where \tilde{B}_{rms} is the rms magnetic field strength, and \tilde{v}_0 and \tilde{l}_0 are the integral speed and scale of the flow. Since \tilde{v}_0 and \tilde{l}_0 remain constant during the collapse, $\tilde{\gamma} = \text{const}$.

The large-scale dynamo (LSD)

The averaged supercomoving induction equation for the mean magnetic field $\langle \tilde{\mathbf{B}} \rangle$ is given by

$$\frac{\partial \langle \tilde{\mathbf{B}} \rangle}{\partial \tilde{t}} = \tilde{\nabla} \times (\langle \tilde{\mathbf{V}} \rangle \times \langle \tilde{\mathbf{B}} \rangle + \tilde{\mathcal{E}} - \eta \tilde{\nabla} \times \langle \tilde{\mathbf{B}} \rangle), \quad (11)$$

where $\tilde{\mathcal{E}} = \langle \tilde{\mathbf{v}} \times \tilde{\boldsymbol{\omega}} \rangle$ and angular brackets denote a suitable averaging (e.g., ensemble or volume averaging or a filtering – see Sect. 7.2 of Ref. [54]). It can be shown that $\tilde{\mathcal{E}} \approx \tilde{\alpha} \tilde{\mathbf{B}} - \tilde{\eta}_t \tilde{\nabla} \times \tilde{\mathbf{B}}$ [6], where $\tilde{\alpha}$ and $\tilde{\eta}_t$ are the turbulent transport coefficients

$$\tilde{\alpha} \approx -\frac{1}{3} \tilde{\tau}_0 \langle \tilde{\mathbf{v}} \cdot \tilde{\boldsymbol{\omega}} \rangle, \quad \tilde{\eta}_t \approx \frac{1}{3} \tilde{\tau}_0 \langle \tilde{\mathbf{v}}^2 \rangle, \quad (12)$$

where $\tilde{\boldsymbol{\omega}} = \tilde{\nabla} \times \tilde{\mathbf{v}}$ and τ_0 is the correlation time of the random flow. Assuming for simplicity that $\langle \tilde{\mathbf{V}} \rangle$ represents a solid-body rotation, the averaged induction equation written in the rotating frame follows as

$$\frac{\partial \langle \tilde{\mathbf{B}} \rangle}{\partial \tilde{t}} = \tilde{\nabla} \times [\tilde{\alpha} \langle \tilde{\mathbf{B}} \rangle \tilde{\eta}_T \tilde{\nabla} \times \langle \tilde{\mathbf{B}} \rangle], \quad (13)$$

with $\tilde{\eta}_T$ introduced in Eq. (9). This type of the turbulent dynamo is known as the α^2 -dynamo. The dependence of the growth rate of the magnetic field on the parameters can be illustrated using the simplest solution of Eq. (13) in infinite space with $\tilde{\alpha}$ and $\tilde{\eta}_T$ independent of time and position (Section 7.5 of Ref. [6] and Ref. [54]),

$$\tilde{\gamma} = \tilde{k} \tilde{\alpha} - \tilde{\eta}_T \tilde{k}^2,$$

where \tilde{k} is the wavenumber of the mean magnetic field. A similar expression is valid for a spherically symmetric distribution of $\tilde{\alpha}$ [54]. The magnetic field of the scale $2\pi/\tilde{k}_m = 4\pi\tilde{\eta}_T/\tilde{\alpha}$ grows most rapidly as $\exp(\tilde{\gamma}_m \tilde{t})$ with $\tilde{\gamma}_m = \tilde{\gamma}(\tilde{k}_m) = \tilde{\alpha}^2/(4\tilde{\eta}_T)$.

Since $\tilde{t} = f(t)$, the magnetic field grows super-exponentially in the physical time. It can be argued that the magnetic field growth rate in physical variables $\gamma_m = \alpha^2/(4\eta_T)$ increases as a decreases but the growth rate in the supercomoving variables $\tilde{\gamma}_m$ remains constant. The supercomoving scale and rms speed of the random flow remain constant during the collapse, $\tilde{l}_0 = l_0/a = \text{const}$ and $\tilde{v}_0 = av_0 = \text{const}$, whereas the correlation time varies as $\tau_0 \approx l_0/v_0 \propto a^2$. This is true at the kinematic stage of the dynamo action since the Lorentz force is negligible and the remaining terms in the supercomoving momentum equation do not include a explicitly. As a result, the mean helicity density of the random flow $\langle \mathbf{v} \cdot \boldsymbol{\omega} \rangle$ increases during the collapse as $\langle \mathbf{v} \cdot \boldsymbol{\omega} \rangle \propto a^{-3}$, while the turbulent magnetic diffusivity remain constant, $\eta_t = \text{const}$. This implies that the growth rate of the physical mean magnetic field varies as $\gamma_m \propto a^{-2}$ (we note that $\eta \ll \eta_t$ under normal conditions, so $\eta_T \approx \eta_t$). Since $d\tilde{t} = dt/a^2$, this implies $\tilde{\gamma}_m = \text{const}$.

THE FORCING FUNCTION

We use the PENCIL CODE forcing function $\tilde{\mathbf{f}}$ written in supercomoving coordinates to generate a random flow in the

simulations [52, 53],

$$\begin{aligned} \tilde{\mathbf{f}}(\tilde{\mathbf{x}}, \tilde{t}) &= \text{Re} \left\{ N \mathbf{f}_{\tilde{\mathbf{k}}(\tilde{t})} \exp \left[i \tilde{\mathbf{k}}(\tilde{t}) \cdot \tilde{\mathbf{x}} + i \phi(\tilde{t}) \right] \right\}, \quad (14) \\ N &= f_0 \tilde{v}_0 \left(\frac{\tilde{k} \tilde{v}_0}{\Delta \tilde{t}} \right)^{1/2}, \quad \mathbf{f}_{\tilde{\mathbf{k}}} = \mathbf{R} \cdot \mathbf{f}_{\tilde{\mathbf{k}}}^{(0)} \\ R_{ij} &= \frac{\delta_{ij} - i\sigma \epsilon_{ijk} \hat{k}_k}{\sqrt{1 + \sigma^2}}, \quad \mathbf{f}_{\tilde{\mathbf{k}}}^{(0)} = \frac{\tilde{\mathbf{k}} \times \mathbf{e}}{\sqrt{\tilde{k}^2 - (\tilde{\mathbf{k}} \cdot \mathbf{e})^2}}, \end{aligned}$$

where $\tilde{\mathbf{k}}$ is the supercomoving wave-vector. The normalization factor N decreases with the time step $\Delta \tilde{t}$ to ensure that the forcing is approximately δ -correlated in the supercomoving time. The time step is calculated using the CFL condition. The remaining factors in N are fixed using dimensional arguments with a dimensionless parameter f_0 to control the forcing strength; we set $f_0 = 1$. The factor σ in R_{ij} is a measure of the kinetic helicity. For SSD we use $\sigma = 0$ to drive a non-helical flow, whereas $\sigma = 1$ for LSD to generate a helical velocity field required to produce a large-scale magnetic field.

DURATION OF THE KINEMATIC STAGE

During the kinematic regime of the SSD in a homologous collapsing background, the physical magnetic field evolves as

$$B = \frac{B_0}{a^2} \exp[\tilde{\gamma} f(t)], \quad (15)$$

where B_0 is the initial field, with the scale factor approximated with

$$a(t) = \left(1 - \frac{t^2}{t_{\text{ff}}^2} \right)^{2/3}, \quad (16)$$

and

$$f(t) = \frac{4t_{\text{ff}}}{\pi} \sqrt{\frac{1-a}{a}}, \quad (17)$$

with t_{ff} the free-fall time and $\tilde{\gamma}$ the growth rate. The time at which kinematic regime ends for the dynamo in a stationary background (the ‘standard’ dynamo) is related to $\tilde{\gamma}$ and B_0 as

$$t_{\text{nl}}^{\text{std}} = \frac{1}{\tilde{\gamma}} \ln \left(\frac{B_{\text{nl}}}{B_0} \right), \quad (18)$$

where B_{nl} is the magnetic field strength at which the Lorentz force becomes sufficiently strong to affect the flow and the magnetic field growth slows down. Substituting Eqs (18) and (17) in Eq. (15), we get

$$\ln \left(\frac{a^2 B_{\text{nl}}}{B_0} \right) = \frac{4}{\pi} \frac{t_{\text{ff}}}{t_{\text{nl}}^{\text{std}}} \sqrt{\frac{1-a}{a}} \ln \left(\frac{B_{\text{nl}}}{B_0} \right). \quad (19)$$

To derive the scale factor, a_{nl} , at which kinematic regime ends for the dynamo in a collapsing background, we compare the left- and right-hand sides of Eq. (19) to obtain the corresponding time t_{nl} using Eq. (16).

For example, consider the amplification of a seed magnetic field by 15 orders of magnitude, $B_{\text{nl}}/B_0 = 10^{15}$ in a cloud with $t_{\text{ff}} = 0.1 t_{\text{nl}}^{\text{std}}$. From Eq. (19), we obtain $a_{\text{nl}} = 0.025$, corresponding to $t_{\text{nl}} = 0.09 t_{\text{nl}}^{\text{std}}$, using Eq. (16). Thus, it takes a ten times shorter time for a dynamo in the collapsing cloud to reach its nonlinear stage than in a stationary background.

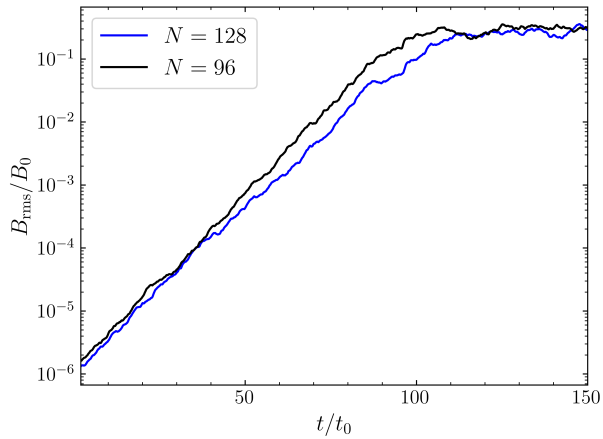


FIG. 1. Comparison of the evolution of B_{rms} in the SSD for the numerical resolutions 128^3 and 96^3 .

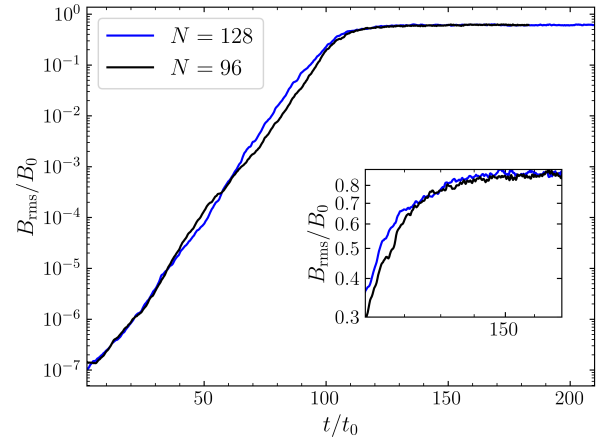


FIG. 2. As Fig. 1 but for the LSD. The inset shows the slow transition to the dynamo saturation completing around $t/t_0 = 160$.

NUMERICAL RESOLUTION TESTS

Here we verify that the numerical resolution of 128^3 is sufficient for our purposes. Figures 1 and 2 show the evolution of the rms physical magnetic field strength B_{rms} in two simulations of SSD and LSD, respectively, with the resolutions 128^3 and 96^3 . The simulation parameters are the same as described in the main text. We find the agreement between the results obtained under the two numerical resolutions to be sufficiently close to justify 128^3 as the resolution used to obtain our main results.